

Zeros, dips and signs in pp and $p\bar{p}$ elastic amplitudes

Flávio Pereira^{1*} and Erasmo Ferreira ^{2*}

¹ *Observatório Nacional, CNPq, Rio de Janeiro 20921-400, RJ, Brazil*

² *Instituto de Física, Universidade Federal do Rio de Janeiro
C.P. 68528, Rio de Janeiro 21945-970, RJ, Brazil*

Abstract

The dips observed in the differential cross sections of elastic pp and $p\bar{p}$ scattering are studied in terms of the locations of the zeros of the real and imaginary parts of the amplitude and of the sign of real part at large $|t|$. It is confirmed that the differences in shapes of the dips in the pp and $p\bar{p}$ systems are determined by a change of sign of the real tail, which seems to be determined by perturbative QCD contributions.

PACS Numbers: 13.85.Dz, 12.38.Lg, 13.85.Lg

* E-mail: flavio@obsn.on.br

* E-mail:erasmo@if.ufrj.br

I. INTRODUCTION

The elastic differential cross sections of pp and $p\bar{p}$ scattering at high energies present a strong forward peak, decreasing exponentially from $|t| = 0$, and forming a dip in the range of values of transferred momentum between 1.3 and 1.5 GeV^2 . For larger values of $|t|$ there is a flatter tail that, for beam energies above 400 GeV ($\sqrt{s} = 27.5 \text{ GeV}$), seems to be independent of the energy.

Chou and Yang [1] studied in an eikonal framework model the hadron-hadron scattering at ultra-high energies, predicting the existence of many dips. Using an impact parameter representation for the scattering amplitude, with a t dependence inspired in the proton electromagnetic form factor, Bourrely, Soffer and Wu [2] were able to reproduce the general features of the ISR experiments. França and Hama [3] described pp scattering under the assumption of a pure imaginary amplitude with two zeros parametrized as a sum of exponentials. With a similar parametrization and including a real part in the amplitude, Carvalho and Menon [4] gave a more detailed representation for pp differential cross sections at the ISR energies. Geometrical models in the eikonal approximation, including the pomeron exchange, were studied by Covelan and collaborators [5]. Extensive descriptions of the phenomenology of the elastic hadron scattering can be seen in the review articles of Bloch and Cahn, and of Jenkovszky [6].

In a somewhat detailed dynamical scheme, Donnachie and Landshoff [7] described the structure of the dip in high energy scattering through the interference of single-pomeron, double-pomeron and three-gluon exchanges, predicting that the dip in $p\bar{p}$ would be less pronounced than in pp scattering.

Table I shows the available data on total cross section, slope parameter B and ratio $\bar{\rho}$ of the forward real to imaginary parts of the amplitudes in pp and $p\bar{p}$ scattering, which come from Fermilab [[8]a,f], CERN-ISR [[8]b,c,d] and CERN-SPS [[8]e]. Most measured differential cross sections [8,9] are limited to $|t| < 10 \text{ GeV}^2$, while large angle data are available only at $\sqrt{s} = 27 \text{ GeV}$ [10], presenting a $|t|$ dependence approximately of the form $|t|^{-8}$ [11], the magnitude of $d\sigma^{el}/dt$ at a given large $|t|$ being nearly energy independent [12]. In measurements of the differential cross section at $\sqrt{s} = 19 \text{ GeV}$ for values of $|t|$ in the range 5 - 12 GeV^2 [10] the data points converge to those of $\sqrt{s} = 27 \text{ GeV}$ for $|t| \approx 11 \text{ GeV}^2$. In order to maintain the universality of the tail we have adopted in our parametrization for all energies between 19 and 63 GeV the same 27 GeV values for large $|t|$.

In this work we explain the detailed shapes of the dips appearing in $d\sigma^{el}/dt$ in terms of the locations of the only one zero of the imaginary part and of the two zeros (in the pp case) of the real part. The amplitudes are obtained from the parametrization [13] of the amplitudes that was inspired in the Model of the Stochastic Vacuum (MSV) [14], with additional freedom in parameters. The differential cross section at large $|t|$ is described through a term in the real part of the amplitude, and a change of sign of this term leads from the pp to the $p\bar{p}$ system, the effect being illustrated by the analysis of the 53 GeV data.

The paper is organized as follows. In Sec. 2 we recall the parametrization used to describe the total and differential cross section data. In Sec. 3 the behavior of the dips of the differential cross section is described in terms of the locations of the zeros of the real

and imaginary amplitudes. Sec. 4 discusses the large $|t|$ behavior of the differential cross section of pp and p \bar{p} systems, and finally in Sec. 5 we present comments and conclusions.

II. PARAMETRIZATION OF THE AMPLITUDES

We use [13] the dimensionless scattering amplitude

$$T(s, t) = 4\sqrt{\pi}s[i\mathcal{I}(t) + \mathcal{R}(t)] , \quad (1)$$

with the elastic differential cross section given by

$$\frac{d\sigma^{el}}{dt} = \frac{1}{16\pi s^2} |T(s, t)|^2 . \quad (2)$$

The imaginary and real parts of the amplitude are respectively parametrized in the forms

$$\mathcal{I}(t) \equiv \alpha_1 e^{-\beta_1|t|} + \alpha_2 e^{-\beta_2|t|} + \lambda 2\rho e^{\rho\gamma} A_\gamma(t) \quad (3)$$

and

$$\mathcal{R}(t) \equiv \alpha'_1 e^{-\beta'_1|t|} + \lambda' 2\rho e^{\rho\gamma'} A_{\gamma'}(t) , \quad (4)$$

where

$$A_\gamma(t) \equiv \frac{e^{-\gamma\sqrt{\rho^2+a^2|t|}}}{\sqrt{\rho^2+a^2|t|}} - e^{\rho\gamma} \frac{e^{-\gamma\sqrt{4\rho^2+a^2|t|}}}{\sqrt{4\rho^2+a^2|t|}} , \quad (5)$$

with $\rho = 3\pi/8$, and we have grouped the factors $2\rho e^{\rho\gamma} A_\gamma(t)$ in order to have $2\rho e^{\rho\gamma} A_\gamma(0) = 1$.

These apparently complicated forms were inspired in the MSV parametrization [13] for the imaginary part of the scattering amplitude. The use of $A_\gamma(t)$ in the real part, has a more convenient structure, compared to simple exponentials, to fill the dip left by the zero of the imaginary part. On the other hand, the simple exponential term $\alpha'_1 \exp(-\beta'_1|t|)$ was included in the real part specifically to describe the large $|t|$ ($5 < |t| < 15 \text{ GeV}^2$) data [10] at 27 GeV. This term is universal (energy independent) for all pp and has opposite sign for p \bar{p} ISR data. The exponential is made numerically equivalent to $|t|^{-8}$ in the $|t|$ range of interest, and was used to avoid the singularity at the origin. This term is not used in the description of the 546 and 1800 GeV data, where large $|t|$ values have not been measured.

At $t = 0$, the optical theorem and the value of $\bar{\rho} = \mathcal{R}(s, 0)/\mathcal{I}(s, 0)$ fix the constraints

$$\mathcal{I}(0) = \alpha_1 + \alpha_2 + \lambda = \frac{\sigma^T}{4\sqrt{\pi}} , \quad (6)$$

and

$$\mathcal{R}(0) = \lambda' + \alpha'_1 = \bar{\rho}(\alpha_1 + \alpha_2 + \lambda). \quad (7)$$

The values of the parameters are given in Table II, which is an update of our previous determination [13], and now includes the $\sqrt{s} = 19.4 \text{ GeV}$ data. The smoothness of the energy dependence of all parameters must be remarked. In comparison to the previous values, the parameters γ and γ' have been slightly modified to improve the description of the data in the region of the dips of the pp differential cross sections as shown in Fig. 1 for $\alpha'_1 > 0$ (solid lines). The case $\alpha'_1 < 0$ (dashed lines), which applies to p \bar{p} scattering, is discussed latter.

III. ZEROS OF THE AMPLITUDES AND DIPS IN pp SCATTERING

The characteristic shape of the dip region of the differential cross sections has been described by Donnachie and Landshoff [7] in terms of various mechanisms of pomeron and gluon exchanges. The low $|t|$ region is described by the single-pomeron exchange (P), which is dominant in this region and gives the value to the slope B . In order to describe the data, the double-pomeron exchange (PP) was introduced with the magnitude of its imaginary part chosen so as to cancel that of the P mechanism in the region where a dip is to be formed. To yield a dip, the real part of the P term is partially cancelled by the three-gluon exchange (ggg), which is dominant for large $|t|$, has opposite signs for pp and $p\bar{p}$ systems, and led to the prediction that at high energies the dips would be less pronounced in $p\bar{p}$ scattering. In addition to these contributions there is the gg (ρ , ω , f , A_2) exchange which is important only at very small $|t|$. We remark that the parametrization given by Eqs. (3) and (4) incorporates all information about the dynamical mechanisms of pp scattering and corresponds to the sum of all terms discussed by Donnachie and Landshoff [7].

According to phenomenological descriptions, the structure of forward pp scattering is determined mainly by the imaginary part of the amplitude which decreases exponentially from $|t| = 0$ and vanishes with a zero located in the interval $|t| = 1.3 - 1.5 \text{ GeV}^2$. This zero is partially filled by the real part of the amplitude which is positive at $|t| = 0$ and also decreases nearly exponentially, becoming negative as $|t|$ reaches $0.2 - 0.3 \text{ GeV}^2$.

Fig. 2 shows the separate contributions $|\text{Im } T(s, t)|^2$ and $|\text{Re } T(s, t)|^2$ to the differential cross section at $\sqrt{s} = 23 \text{ GeV}$. The real part in pp scattering (dashed line) has two zeros, becoming negative in the region between them. The zero of $\text{Im } T(s, t)$ (solid line) is situated between the two zeros of $\text{Re } T(s, t)$.

This description is valid for all energies of pp scattering from 19 to 63 GeV. The zeros of the real and imaginary parts of the pp amplitude as a function of the energy are shown in Fig. 3. The position of the zeros of $\text{Im } T(s, t)$ and the first zeros of $\text{Re } T(s, t)$ decrease monotonically with the energy, while that of the second zero of $\text{Re } T(s, t)$ oscillates, being lowest at about 30 GeV, as shown in Fig. 3. The position of the dips in the differential cross sections are always situated between the zeros of $\text{Im } T(s, t)$ and the second zeros of $\text{Re } T(s, t)$. The dips are close to the zeros of $\text{Im } T(s, t)$, but the shapes in the dip region are strongly influenced by the distance between the zeros of $\text{Im } T(s, t)$ and $\text{Re } T(s, t)$. At about 30 GeV they are closest, and correspondingly the dips are remarkably pronounced (narrow and deep), as can be seen in Fig. 1 (solid lines), where the changes in the form and position of the dips in the interval 19 - 63 GeV are exhibited in an extended scale.

A similar behavior is also shown by the magnitudes of the differential cross sections at the dip. Fig. 4 shows the minimum values of $d\sigma^{\text{el}}/dt$ as a function of \sqrt{s} , the lowest dip occurring at 30 GeV. The values at 546 and 1800 GeV must be understood only as estimates, while at 630 GeV [[8]e] the dip is clearly seen in the data.

IV. SIGNS OF THE LARGE ANGLE pp AND $p\bar{p}$ AMPLITUDES

Donnachie and Landshoff observed that the quasi- $|t|^{-8}$ dependence of $d\sigma^{el}/dt$ at large $|t|$ observed experimentally can be described by a three-gluon exchange mechanism, which is energy independent [11]. Other terms contributing to the amplitude are the two-gluon-one-pomeron exchanges (ggP) and three pomeron exchanges (PPP). The $A_{ggP}(s, t)$ and $A_{PPP}(s, t)$ terms have very little effect for the amplitude $A(s, t) = A_{ggg}(s, t) + A_{ggP}(s, t) + A_{PPP}(s, t)$, the dominant term at large $|t|$ being $A_{ggg}(s, t)$. This term has the form

$$A_{ggg}(s, t) = -\frac{N}{|t|} \frac{5}{54} \left[4\pi\alpha_s(|\hat{t}|) \frac{1}{m^2(|\hat{t}|) + |\hat{t}|} \right]^3, \quad (8)$$

where $m^2(|\hat{t}|)$ is an effective gluon mass, $\alpha_s(|\hat{t}|)$ is the running coupling constant, $\hat{t} \simeq t/9$, $\Lambda = 200$ MeV and $m_0 = 340$ MeV and for $\hat{t} \gg 1$ yields the $|t|^{-8}$ dependence of the large $|t|$ differential cross section. The normalization factor N is negative and determined by the proton wave function.

To avoid the non regular behavior at small $|t|$, we use in the real amplitude an exponential form $\alpha'_1 \exp(-\beta'_1 |t|)$ rather than a negative power $|t|^{-8}$ to reproduce the tail. This term describes the large $|t|$ behavior at 53 GeV where both pp and $p\bar{p}$ differential cross sections have been measured beyond the dip region. To show the effect of the sign of the first term in Eq.(4), in Fig. 1 we disregard the differences in the experimental values of σ^T , B and $\bar{\rho}$ for pp and $p\bar{p}$ systems and also keep the numerical values of all parameters of the real and imaginary parts of the amplitude, only changing the sign of α'_1 in Eq. (4). Fig. 1 shows the effects of this change of sign in the dip region, with the dashed lines for $\alpha'_1 < 0$ representing $p\bar{p}$ scattering.

Fig. 5 shows $d\sigma^{el}/dt$ for pp ($\alpha'_1 > 0$) and $p\bar{p}$ ($\alpha'_1 < 0$) scattering at 53 GeV, where we have used, in the constraint imposed through Eq. (7), the realistic values of $\bar{\rho}$ given for each case in Table I. The $p\bar{p}$ dip is less deep, and becomes still flatter as the energy increases. The explanation for this behavior in terms of the zeros of the amplitudes is shown in Fig. 2. The real part of the amplitude with a positive tail ($\alpha'_1 > 0$) presents two zeros, the zero near the origin having no influence in the dip region. The second zero, which is close to the zero of the imaginary part (solid line) is responsible for the pronounced form of the dip. Changing the sign of α'_1 , the second zero does not exist (or it would be located very far away). The change of sign in α'_1 makes, in the region of the dip, the $(-)$ line higher than the $(+)$ line, flattening the dips.

V. COMMENTS AND CONCLUSIONS

In the present work, starting from a parametrization [13] suggested by the Model of the Stochastic Vacuum [14], we relate the behavior of the dips of the elastic differential cross section to the locations of the zeros of the amplitudes in pp and $p\bar{p}$ scattering, and investigate the role of the sign of the large $|t|$ tail for these systems, in the range $\sqrt{s}=19 - 63$ GeV.

The pp amplitude presents one zero in the imaginary part and two zeros in the real part. The depth of the dips is determined by the proximity between the zeros of the imaginary

part and the second zeros of the real part, so that the dips become deeper when these zeros are closer to each other. In $p\bar{p}$ scattering the real amplitude has only the first zero, which occurs far away from the dip region.

The large $|t|$ tail of the differential cross section is described by an exponential term included in the real part of the amplitude. This term, which is the same (except for a sign) for pp and $p\bar{p}$ at all energies from 19 to 63 GeV, is responsible for the change of shape of the dip region when we change from pp to $p\bar{p}$ systems. The sign (which is positive for pp scattering) determines flatter dips in $p\bar{p}$ scattering. This fact, which was pointed out by Donnachie and Landshoff [7], is here confirmed by the detailed description of all data.

Our parametrization describes all data in detail and has a remarkably smooth behavior that allows interpolations for predictions.

ACKNOWLEDGMENTS

The authors wish to thank M. J. Menon, A. F. Martini and P. A. Carvalho for information on their work.

REFERENCES

- [1] T. T. Chou and C. N. Yang, Phys. Rev. **D19**, 3268 (1979).
- [2] C. Bourrely, J. Soffer and T.T. Wu, Phys. Rev. **D19**, 3249 (1979); Nucl. Phys. **B247**, 15 (1984); Phys. Lett. **B252**, 287 (1990); *ibid.* **B315**, 195 (1993).
- [3] H. M. França and Y. Hama, Phys. Rev. **D19**, 3261 (1979).
- [4] P.A. Carvalho and M. Menon, Phys. Rev. **D56**, 7321 (1997).
- [5] R. J. M. Covolan *et al.*, Z. Phys. **C51**, 459 (1991); Nucl. Phys. B (Proc. Suppl.) **25B**, 86 (1992); Z. Phys. **C58**, 109 (1993); Phys. Lett. **B389**, 176 (1996).
- [6] M. M. Bloch and R. N. Cahn, Rev. Mod. Phys. **57**, 563 (1985); L. L. Jenkovszky, Fortschr. Phys. **34**, 791 (1986).
- [7] A. Donnachie and P.V. Landshoff, Phys. Lett. **123B**, 345 (1983); Nucl. Phys. **B231**, 189 (1984).
- [8] Data on pp and $\bar{p}p$ systems. (a) A. S. Carrol *et al.*, Phys. Rev. Lett. **33**, 928 (1974); A. Schiz *et al.*, Phys. Rev. **D24**, 26 (1981). L. A. Fajardo *et al.*, Phys. Rev. **D24**, 46 (1981); R. L. Cool *et al.*, Phys. Rev. **D24**, 2821 (1981); R. Rubinstein *et al.*, Phys. Rev. **D30**, 1413 (1984); (b) N. Amos *et al.*, Nucl. Phys. **B262**, 689 (1985); (c) R. Castaldi and G. Sanguinetti, Ann. Rev. Nucl. Part. Sci. **35**, 351 (1985); (d) U. Amaldi and K.R. Schubert, Nucl. Phys. **B166**, 301 (1980). (e) D. Bernard *et al.*, Phys. Lett. **B171**, 142 (1986); C. Augier *et al.*, Phys. Lett. **B316**, 448 (1993); G. Fidecaro *et al.*, Phys. Lett. **105B**, 309 (1981); (f) N. Amos *et al.*, Phys. Lett. **B243**, 158 (1990); N. Amos *et al.*, *ibid.* **B247**, 127 (1990); Phys. Rev. Lett. **68**, 2433 (1992).
- [9] E. Nagy *et al.*, Nucl. Phys. **B150**, 221 (1979); K.R. Schubert, *Tables on Nucleon-Nucleon Scattering*, in Landolt-Börnstein *Numerical data and Functional Relationships in Science and Technology*, New Series, vol.I/9a (1979); A. Breakstone *et al.*, Nucl. Phys. **B248**, 253 (1984); Phys. Rev. Lett. **54**, 2180 (1985).
- [10] W. Faissler *et al.*, Phys. Rev. **D23**, 33 (1981).
- [11] A. Donnachie and P.V. Landshoff, Z. Phys. **C2**, 55 (1979); Phys. Lett. **B387**, 637 (1996).
- [12] S. Conetti *et al.*, Phys. Rev. Lett. **41**, 924 (1978).
- [13] Pereira, F. and E. Ferreira, Phys. Rev. **D58**, 014008-1 (1999).
- [14] H.G. Dosch, E. Ferreira and A. Krämer, Phys. Lett. **B289**, 153 (1992); *ibid.* **B318**, 197 (1993); Phys. Rev. **D50**, 1992 (1994).

FIGURES

FIG. 1. Fittings of elastic differential cross sections through Eqs.(3) and (4) at 19.4 GeV and ISR energies, shown in an extended scale only in the region of the dips of pp scattering with $\alpha'_1 > 0$ (solid lines) and the predictions for $p\bar{p}$ scattering with $\alpha'_1 < 0$ (dashed lines). Curves and data at different energies are conveniently separated through multiplication by powers of 10.

FIG. 2. Separate contributions of $|\text{Im } T|^2$ and $|\text{Re } T|^2$ for $d\sigma^{el}/dt$ at 23.5 GeV. The dip in the data at about 1.5 GeV^2 is due to a zero in $\text{Im } T$. The real part (dashed line) is positive at $|t| = 0$, becomes negative at small $|t|$ and fills partially the zero of $\text{Im } T$ that produces the dip. The dotted line represents the squared tail term $\alpha'_1 \exp(-\beta'_1 |t|)$ alone. If this term is positive, it causes a second zero, as shown by the (+) line. In the (−) line the tail is negative and no second zero of $\text{Re } T$ exists, lowering the depth of the dip.

FIG. 3. Locations of the zeros of the imaginary and real parts of the scattering amplitude (white squares) and the positions of the dips of $d\sigma^{el}/dt$ (black squares) as functions of energy.

FIG. 4. Energy dependence of the values of the elastic differential cross section at the bottom of the dips.

FIG. 5. Results for the elastic differential cross section at 53 GeV through Eq. (3) and (4) with $\alpha'_1 > 0$ (pp) and $\alpha'_1 < 0$ ($p\bar{p}$), and with the experimental values of $\bar{\rho}$ used in Eq.(7) for each case. The pp data and the solid curve are multiplied by 10^{-1} .

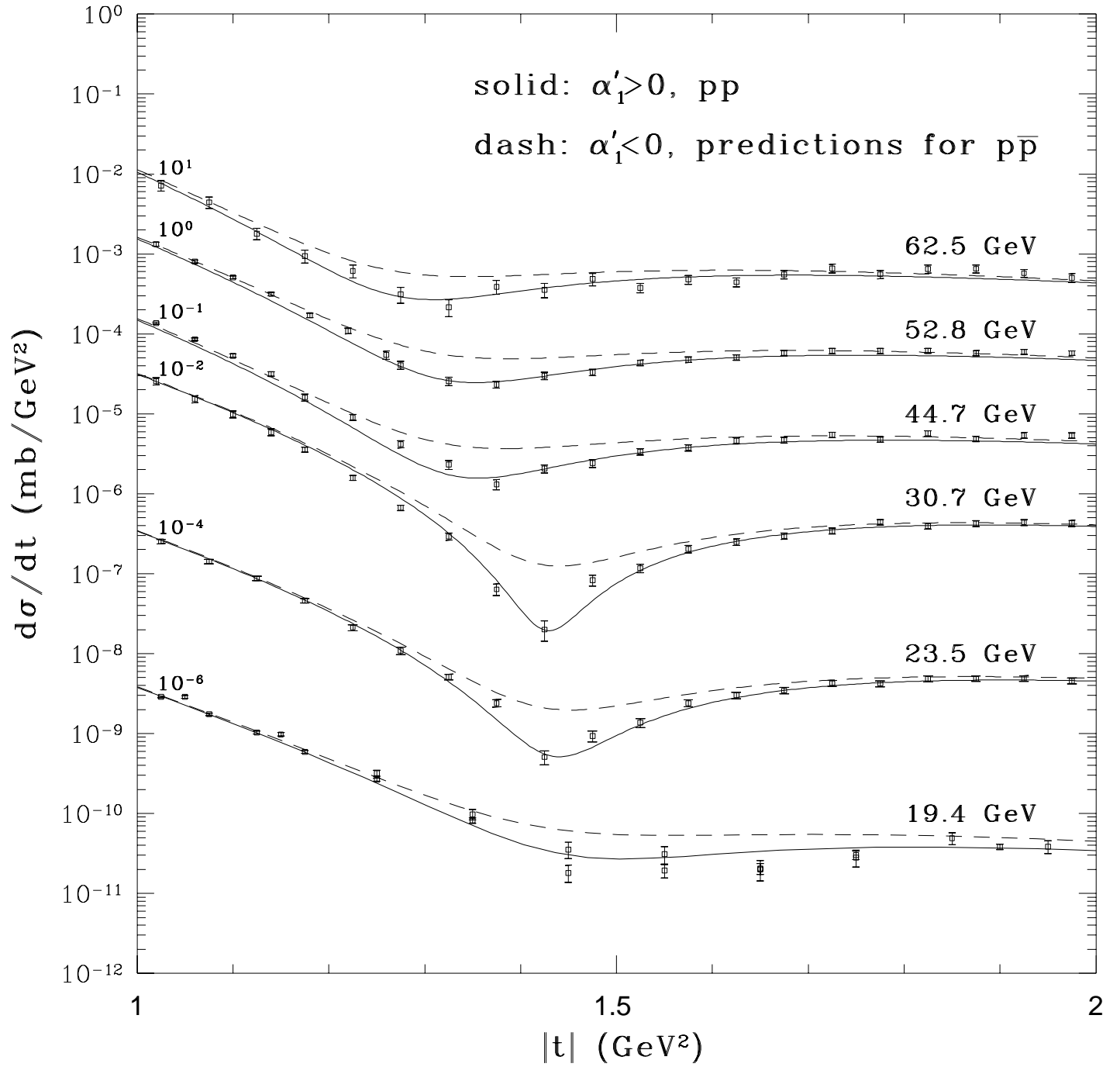
TABLES

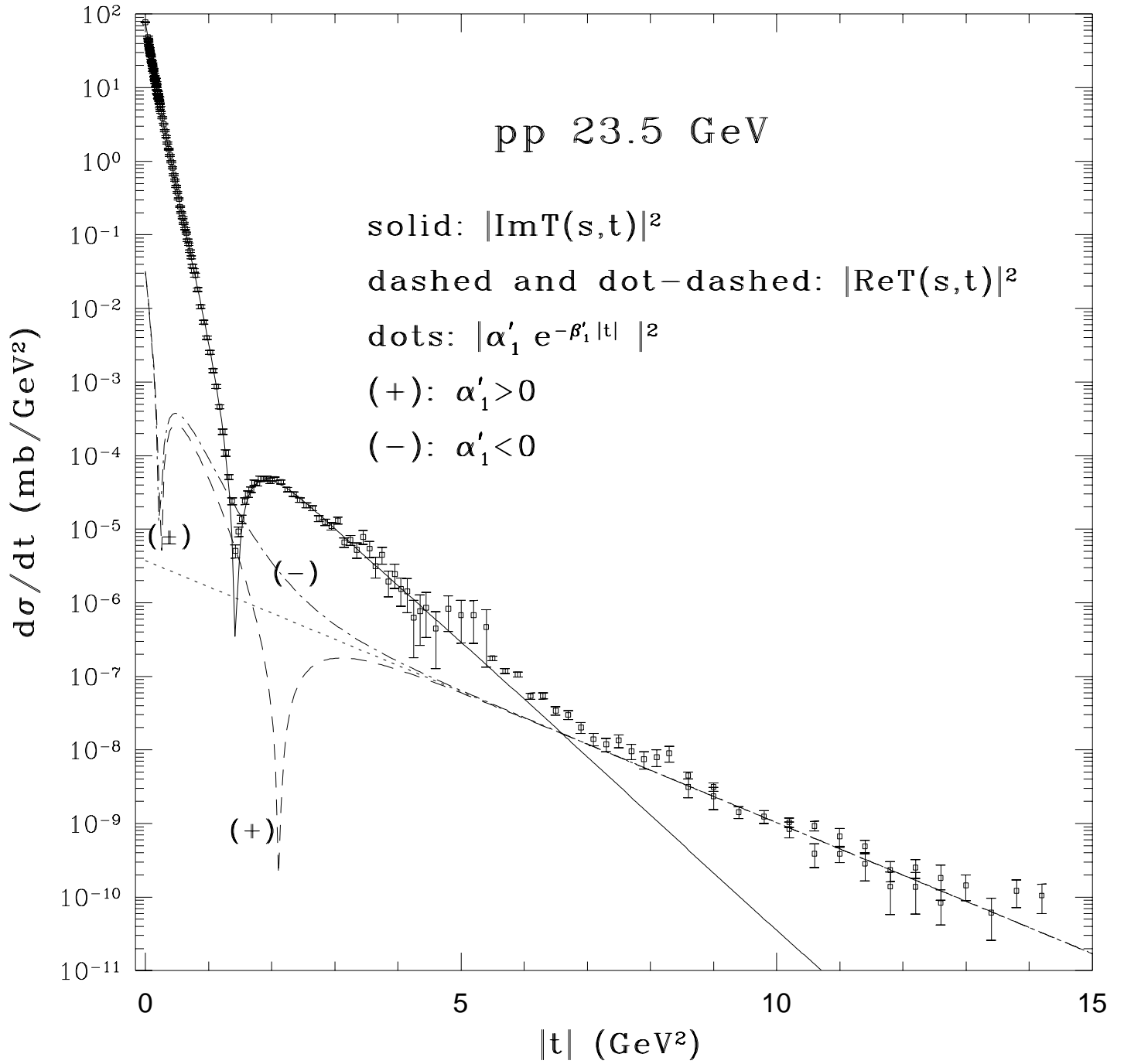
TABLE I. Experimental Data

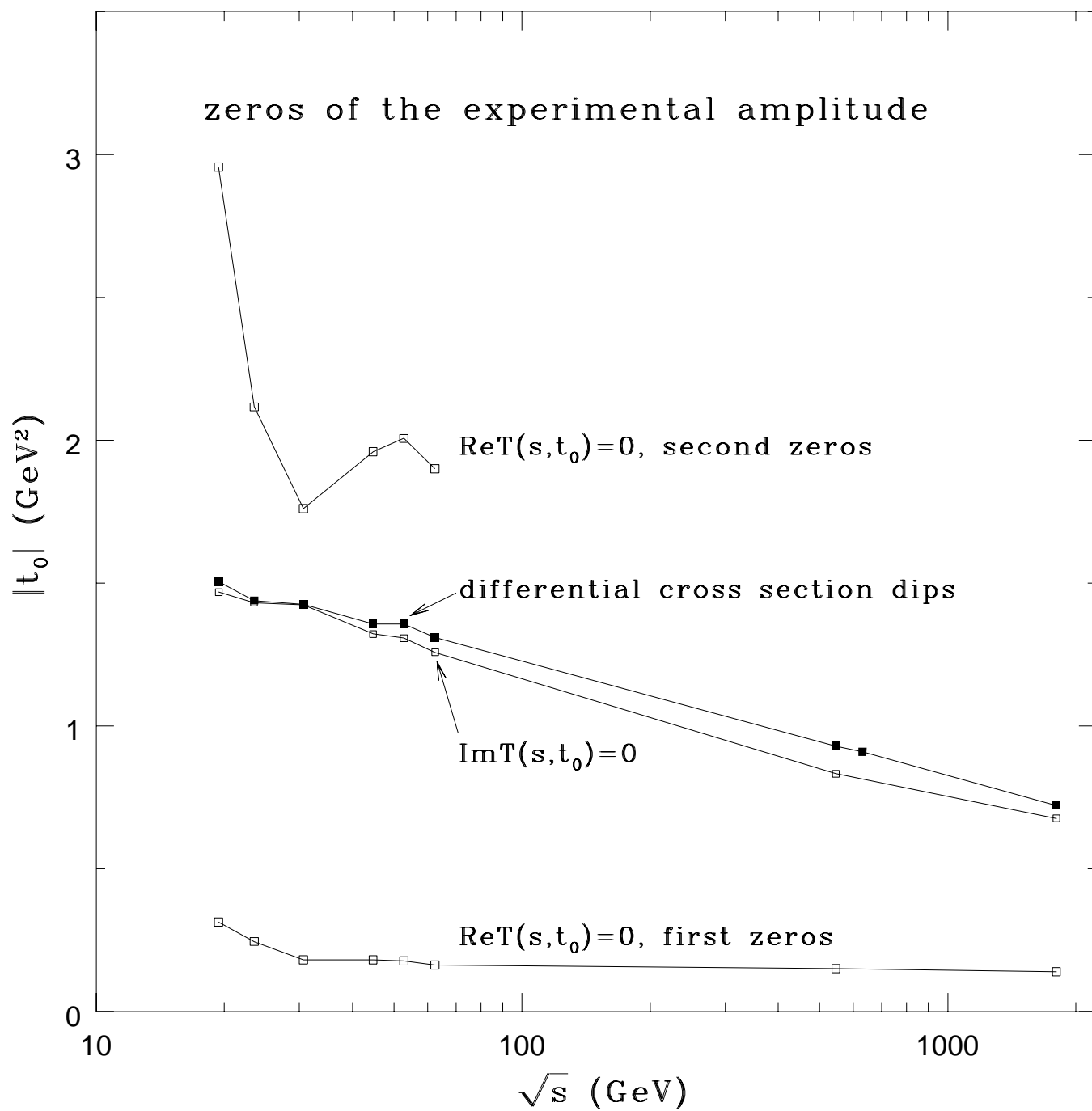
	\sqrt{s} (GeV)	σ^T (mb)	B (GeV ⁻²)	Ref. [8]	$\bar{\rho}$	Ref. [8]
pp	19.4	38.97 ± 0.06	11.74 ± 0.04	(a)	0.019 ± 0.016	(a)
	23.5	39.65 ± 0.22	11.80 ± 0.30	(b)	0.020 ± 0.050	(c, d)
	30.7	40.11 ± 0.17	12.20 ± 0.30	(b)	0.042 ± 0.011	(c, d)
	44.7	41.79 ± 0.16	12.80 ± 0.20	(c)	0.062 ± 0.011	(c, d)
	52.8	42.38 ± 0.15	12.87 ± 0.14	(b)	0.078 ± 0.010	(c, d)
	62.5	43.55 ± 0.31	13.02 ± 0.27	(b)	0.095 ± 0.011	(c, d)
$\bar{p}p$	52.8	43.32 ± 0.34	13.03 ± 0.52	(b)	0.106 ± 0.016	(b, c)
	541	62.20 ± 1.50	15.52 ± 0.07	(e)	0.135 ± 0.015	(e)
	1800	72.20 ± 2.70	16.72 ± 0.44	(f)	0.140 ± 0.069	(f)

TABLE II. Values of parameters for Eqs. (3) and (4). $\alpha_1, \beta_1, \alpha_2, \beta_2, \lambda$ and λ' are in GeV⁻², and γ, γ' are dimensionless. $\alpha'_1 = 0.0031$ GeV⁻² and $\beta'_1 = 0.41$ GeV⁻² are the same for all ISR energies and 19.4 GeV.

\sqrt{s}	α_1	β_1	α_2	β_2	λ	λ'	γ	γ'	χ^2
19.4	1.7400	1.3398	2.8771	2.2098	9.4000	0.2632	3.7019	3.67	3.53
23.5	1.7298	1.4390	3.1091	2.2949	9.1850	0.2774	3.8625	5.00	1.18
30.7	1.8224	1.4502	3.1649	2.3299	9.5467	0.6073	3.9015	6.70	1.33
44.7	1.6699	1.5025	3.0000	2.1086	10.3650	0.9354	4.0306	6.65	4.36
52.8	1.8500	1.5287	2.9600	2.1753	10.4630	1.1913	4.0529	6.80	3.29
62.5	1.9272	1.5529	2.8081	2.1337	10.8201	1.4747	4.0921	7.35	1.76
546	2.6174	2.1539	3.9061	2.1813	15.7463	3.0270	4.8190	7.97	1.23
1800	3.1036	2.4526	4.4246	2.4253	18.3315	3.6204	5.3450	8.60	2.00







minimum values of $\frac{d\sigma}{dt}$

